

# Path-reversed substrate-guided-wave optical interconnects for wavelength-division demultiplexing

Jian Liu and Ray T. Chen

A path-reversed substrate-guided-wave holographic interconnection scheme is investigated for a wavelength-division demultiplexing application. Using a beveled edge of a waveguiding plate allows optical signals to be coupled into the waveguiding plate and then to be coupled out of the plate by a waveguide hologram. Theoretical analyses are given for dispersion, bandwidth, and recording parameters of various guided-wave holographic gratings. A device is fabricated with a 45° incident angle and a 45° diffraction angle by use of a 20- $\mu\text{m}$  photopolymer film. The 3-dB bandwidth of the device is measured to be 20 nm. Four-channel wavelength demultiplexing is demonstrated at 796, 798, 800, and 802 nm with no cross talk observed. A one-to-five cascaded four-channel wavelength-division demultiplexer with  $\pm 5\%$  energy uniformity under *s* polarization is also demonstrated to increase the user-sharing capacity. Twenty fan-out channels ( $5 \times 4$ ) are achieved experimentally. © 1999 Optical Society of America

*OCIS codes:* 050.1970, 090.0090, 060.2360, 060.4230, 060.4250.

## 1. Introduction

Photopolymer films have been demonstrated to be an efficient material for making holographic gratings. Photopolymer-based holograms have been applied in optical storage,<sup>1</sup> optical correlators,<sup>2</sup> Fourier transforms,<sup>3</sup> optical computing,<sup>4</sup> optical back planes,<sup>5</sup> and optical communication networks.<sup>6–8</sup> In this paper we propose a novel path-reversed substrate-guided-wave optical interconnect scheme functioning as a wavelength-division demultiplexer (WDDM) for separating optical channels with different wavelengths.

In optical communications a wavelength-division multiplexer (WDM) provides a powerful approach to increasing the capacity of the fiber transmission lines significantly. At the end of a transmission line a WDDM is always employed to separate optical channels of different wavelengths and to route optical signals to their designated users. For long-haul telecommunications at wavelengths of 1330 and 1550

nm, investigators have focused on two kinds of grating-based approaches: arrayed-waveguide gratings<sup>9–14</sup> and fiber Bragg gratings.<sup>15–19</sup> Dispersion in arrayed-waveguide gratings is caused by the difference in length of the arrayed waveguides. The wavelength selectivity of a fiber Bragg grating is due to a relatively long fiber grating with low refractive-index modulation. In data communications in which the interconnection distance is relatively short, usually within 1 km, it is better to use short wavelengths, for example 800 nm, in conjunction with a multimode fiber to transmit optical signals. In this situation, optical transceivers are mature, and the aggregate bandwidth can meet the system requirements.<sup>20–24</sup> Substrate-guided-wave holographic-grating-based WDDM's show promise.<sup>8,25</sup> In this paper we present a path-reversed substrate-guided-wave optical interconnect for wavelength-division demultiplexing centered at a wavelength of 800 nm.

For previous substrate-guided-wave holograms<sup>8,25</sup> optical signals of various wavelengths were dispersed by an input holographic grating, propagated within a waveguiding plate with total internal reflection, and then coupled out of the substrate by output holographic gratings. The interchannel wavelength separation of such a WDDM is completely dependent on the length between the input and the output couplers. To obtain a smaller channel wavelength spacing, it is necessary to employ a long substrate.

---

The authors are with the Microelectronics Research Center, Department of Electrical and Computer Engineering, University of Texas at Austin, Austin, Texas 78758. R. Chen's e-mail address is raychen@uts.cc.utexas.edu.

Received 31 July 1998; revised manuscript received 3 December 1998.

0003-6935/99/143046-07\$15.00/0

© 1999 Optical Society of America

Meanwhile, a lens array is always needed to couple the output optical signals of different wavelengths into a fiber array. In our proposed path-reversed substrate-guided-wave optical interconnect, instead of an input holographic grating, a beveled edge is used to couple optical signals into the waveguiding plate with an angle larger than the critical angle of the plate. Also, a photopolymer-based holographic grating is employed to separate the optical signals of different wavelengths. It is a path-reversed structure because the optical signals are dispersed by the output waveguide hologram for which the input light comes from the waveguiding plate and the diffracted light goes into the air. Only one lens can be used to couple the dispersed optical signals into their designated fibers. Moreover, multiple fan-outs can be realized by the integration of a cascaded holographic-grating array on the same waveguiding plate.

In this paper Section 2 describes the dispersion, bandwidth, and recording parameters of the guided-wave holographic gratings. Experimental results showing a four-channel WDDM and a multiple-fan-out configuration are given in Section 3. Concluding remarks are given in Section 4.

## 2. Working Principles

### A. Photopolymer Films

DuPont photopolymers (DuPont Holographic Materials, Wilmington, Delaware) are promising as holographic films because of their dry-processing capacity, long shelf life, good photospeed, and high index modulation.<sup>26-29</sup> The holographic photopolymer is usually coated in the solvent state onto a clear support, typically a Mylar polyester film. A removable cover sheet is used as a protective cover. The available thicknesses of the photopolymers are from 10 to 100  $\mu\text{m}$ . The hologram-formation mechanism in the photopolymer films is known to be a three-step process. First, exposure initiates an interference pattern, which causes the initial polymerization and the diffusion of the monomer molecules to bright fringe areas from dark fringe neighborhoods in the photopolymer. A higher concentration of polymerization means a higher refractive index. Second, uniform UV light is required for bleaching the dye and complete polymerization. Third, a baking process further enhances the refractive-index modulation of the hologram formed in the photopolymer film. It is shown that the dynamic properties of the diffraction efficiency versus the exposure time can be controlled by the two recording-beam intensities, which are related to the polymerization and the diffusion rates in the photopolymer films.<sup>27</sup> In our experiment photopolymer HRF 600 $\times$ 001-20 (20  $\mu\text{m}$  thick) was selected as the recording material because it exhibits lower scattering and a higher diffraction efficiency.<sup>29</sup>

### B. Dispersion and Bandwidth of the Path-Reversed Substrate-Guided-Wave Holograms

Figure 1 shows the structure of the proposed path-

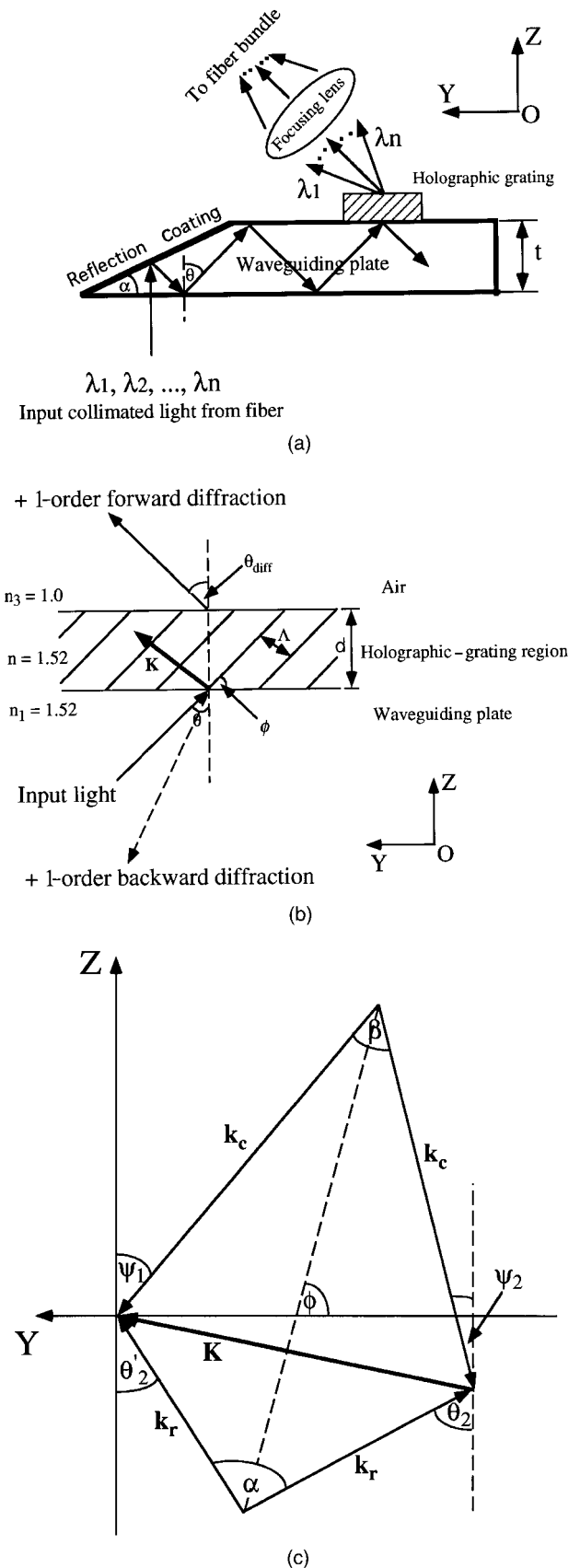


Fig. 1. Path-reversed substrate-guided wave optical interconnection: (a) structure, (b) guided-wave holographic grating, (c) phase-matching condition for the recording and the reconstruction of the grating.

reversed substrate-guided-wave interconnect. Collimated optical signals of different wavelengths are coupled into a waveguiding plate with an aluminum-coated beveled edge with an angle  $\alpha$ , zigzag within the substrate with a bounce angle larger than the critical angle of the waveguiding plate, and then are coupled out by the photopolymer-based volume holographic grating that is fabricated on one side of the substrate. The dispersed optical signals can be coupled by a focusing lens into a fiber array. The thickness of the waveguiding plate is  $t$ . Figure 1(b) shows the detailed structure of a volume holographic grating with a thickness  $d$ . The grating has a period  $\Lambda$  and a slanted angle  $\phi$ . The grating equation is given by<sup>30</sup>

$$\Lambda_y(\sin \theta_2' + \sin \theta_2) = m\lambda/n, \quad m = 0, \pm 1, \pm 2, \dots, \quad (1)$$

where  $\theta_2$  and  $\theta_2'$  are the incident angle and the diffraction angle, respectively, of the optical signals in the holographic-grating region at the center wavelength of  $\lambda$  (in air),  $n$  is the average refractive index of the holographic-grating region,  $\Lambda_y = \Lambda/\sin \phi$  is the grating period projected in the  $Y$  direction, and  $m$  represents the  $m$ th order for forward diffraction. In our case  $m$  is equal to 1. Let  $\theta_{\text{diff}}$  be the designed diffraction angle in air with a refractive index  $n_3$ , and let  $\theta$  be the bounce angle, i.e., the incident angle at the interface between the waveguiding plate and the grating. From the geometry shown for the beveled edge, we have  $\theta = 2\alpha$ .

The dispersion of the grating can be derived by the differentiation of Eq. (1), which yields

$$\begin{aligned} d\theta_{\text{diff}}/d\lambda &= \sin \phi / \Lambda \cos \theta_{\text{diff}} \\ &= n(\sin \theta_2' + \sin \theta_2) / \lambda \cos \theta_{\text{diff}}. \end{aligned} \quad (2)$$

From the geometry shown in Fig. 1(c) the slanted angle  $\phi$  of the grating and the grating period  $\Lambda$  are given by

$$\phi = \pi/2 + (\theta_2' - \theta_2)/2, \quad (3)$$

$$\Lambda = \lambda/2n \sin[(\theta_2' + \theta_2)/2], \quad (4)$$

respectively, where  $\theta_2'$  and  $\theta_2$  are calculated from the design values of  $\theta_{\text{diff}}$  and  $\theta$ , respectively, by use of Snell's law.

Figure 2(a) shows plots of the grating dispersion as a function of the diffraction angle at incident angles of  $0^\circ$ ,  $30^\circ$ ,  $45^\circ$ ,  $60^\circ$ , and  $75^\circ$  by use of Eq. (2) at a center wavelength of 800 nm. The incident angles of  $0^\circ$  and  $30^\circ$  are also plotted in Fig. 2 for comparison. The thickness of the guided-wave holographic gratings is 20  $\mu\text{m}$ . The refractive indices are  $n_1 = 1.0$  and  $n = n_3 = 1.52$ . It can be seen that higher dispersion occurs for a grating with a higher incident angle and a higher diffraction angle.

In the design of a WDDM with a dispersion grating the spectral bandwidth of the grating has to accommodate all wavelength channels that are demulti-

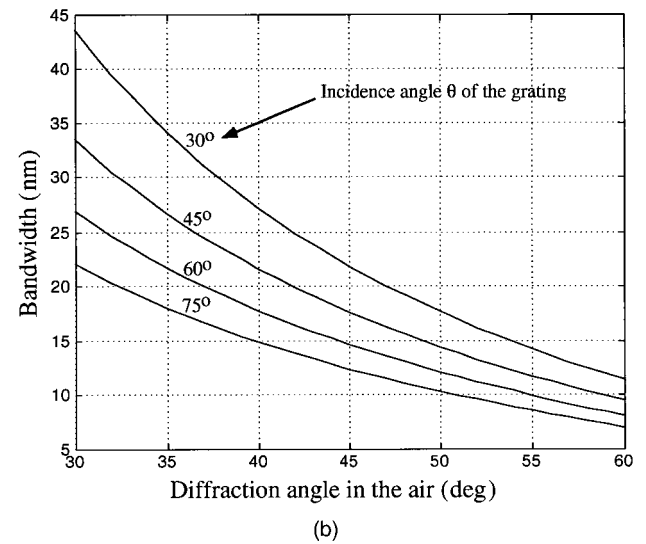
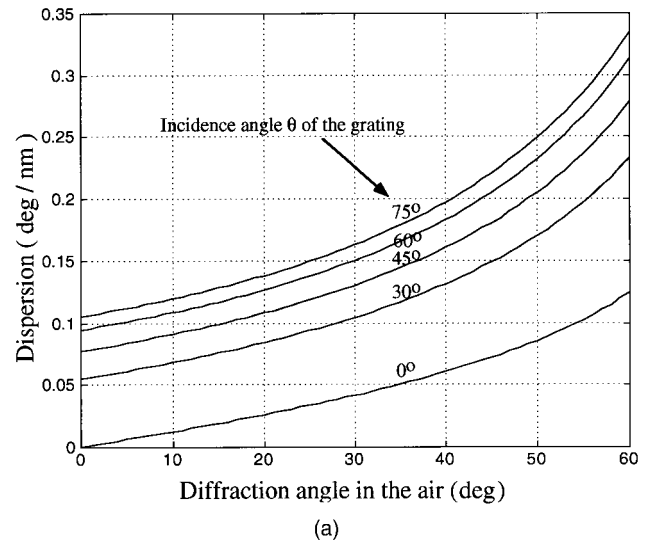


Fig. 2. (a) Dispersion as calculated with Eq. (2) and (b) bandwidth calculated with Eq. (5).

plexed. The approximate spectral bandwidth is given by Ludman<sup>31</sup> in the form of

$$\frac{\Delta\lambda}{\lambda} = \frac{\Lambda \cos \theta_2' \sin \phi}{d \sin \theta_2'}, \quad (5)$$

which is plotted in Fig. 2(b). Table 1 shows the calculated parameters for four guided-wave grating structures. There exists a trade-off between the dispersion and the bandwidth of the guided-wave holographic gratings.

Table 1. Parameters for Four Guided-Wave Holographic Gratings

Case	$\alpha$	$\theta$	$\theta_{\text{diff}}$	$\Lambda$	$\phi$	$d\theta_{\text{diff}}/d\lambda$	Bandwidth
1	$22.5^\circ$	$45^\circ$	$30^\circ$	495.2 nm	$77.1^\circ$	0.13	33 dB
2	$22.5^\circ$	$45^\circ$	$45^\circ$	444.6 nm	$81.4^\circ$	0.18	18 dB
3	$22.5^\circ$	$45^\circ$	$60^\circ$	411.2 nm	$84.9^\circ$	0.28	9.4 dB
4	$30^\circ$	$60^\circ$	$60^\circ$	358.3 nm	$77.4^\circ$	0.31	8.1 dB

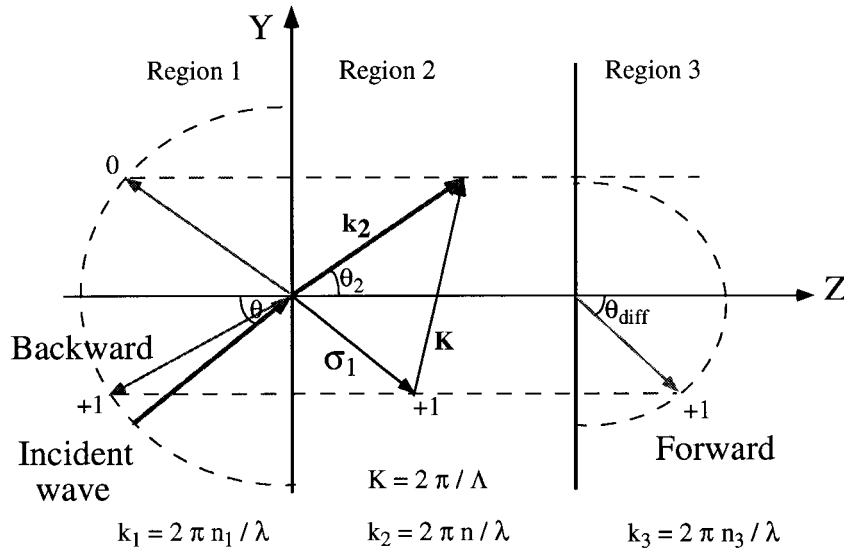


Fig. 3. Conceptual interpretation of forward and backward diffraction by rigorous coupled-wave analysis. Regions 1, 2, and 3 refer to the waveguiding plate, the grating, and air, respectively, as shown in Fig. 1;  $k_1$ ,  $k_2$ , and  $k_3$  are the amplitudes of the three wave vectors in these three media (semicircles with these radii are shown in regions 1 and 3). The wave vectors  $\sigma_i$  of the decomposed inhomogeneous plane waves in region 2 are given by the vector Floquet condition. The allowed wave vectors in regions 1 and 3 must be phase matched to the boundary components (along the  $Y$  direction) of these decomposed wave vectors. The horizontal dashed lines show such restrictions.

### C. Hologram-Recording Parameters

Figure 1(c) shows a phase-matching diagram for the recording and the reconstruction wave vectors in the holographic medium for the +1-order Bragg diffraction.<sup>30,32</sup> The recording wave vector  $\mathbf{k}_c$  ( $|\mathbf{k}_c| = 2\pi n'/\lambda_c$ ) is phase matched with grating vector  $\mathbf{K}$  ( $|\mathbf{K}| = 2\pi/\Lambda$ ), as are the reconstruction wave vector  $\mathbf{k}_r$  ( $|\mathbf{k}_r| = 2\pi n/\lambda$ ) and  $\mathbf{K}$ . The term  $n'$  is the average refractive index of the guided-wave holographic emulsion at the recording wavelength  $\lambda_c$ . From the geometry shown in Fig. 1(c) the recording angles in the holographic medium of the two recording beams of wavelength  $\lambda_c$  are derived and given by

$$\psi_1 = \frac{\pi}{2} - \left( \phi - \frac{\beta}{2} \right), \quad (6)$$

$$\psi_2 = \left( \phi + \frac{\beta}{2} \right) - \frac{\pi}{2}, \quad (7)$$

where

$$\beta = 2 \sin^{-1} \left\{ \left( \frac{n\lambda_c}{n'\lambda} \right) \sin \left[ \frac{(\theta_2' + \theta_2)}{2} \right] \right\}, \quad (8)$$

which is the angle between the two recording beams. Note that the phase-matching condition of Fig. 1(c) is in the holographic medium. In practice, the recording angles calculated with Eqs. (6) and (7) must be converted into their corresponding angles in air by use of Snell's law.

It is obvious that the absolute values of the two recording angles in air cannot be greater than  $90^\circ$ . Otherwise, a prism must be used to obtain the required interference in the holographic medium, which always deteriorates the quality of the record-

ing beams. Among the four cases shown in Table 1, case 2 has a reasonably high dispersion and an acceptable bandwidth. Moreover, this kind of structure is easy to fabricate. By changing the center wavelength of 800 nm, we can obtain the grating structures operating at 1550 nm.

### 3. Experiment

We use a 514-nm argon-ion laser to record the output holographic grating. The reconstruction wavelength is designed to be 800 nm. A Ti:sapphire tunable laser is employed to characterize the performance of the device. The DuPont photopolymer film HRF 600×001-20 with a thickness of 20  $\mu\text{m}$  is chosen for recording the guided-wave holographic grating. The waveguiding plate has a thickness of 6.3 mm. The beveled angle  $\alpha$  is  $22.5^\circ$ , and the diffraction angle  $\theta_{\text{diff}}$  in air is  $45^\circ$ .

In our experiment +1-order backward diffraction is observed to be approximately 15% of the intensity of the +1-order forward diffraction, which can be interpreted by use of rigorous coupled-wave analysis,<sup>33</sup> as is depicted conceptually in Fig. 3. The decomposed space-harmonic components of the total field in the grating region that are coupled into the glass-plate region (backward diffraction) and air (forward diffraction) include a +1-order forward diffraction and a +1-order backward diffraction. Other diffraction orders are cut off outside the grating region. It can be seen from Fig. 3 that backward diffraction orders always exist as long as forward diffraction orders exist because of the larger refractive index in region 1 (the waveguiding region). The existing +1-order backward diffraction takes a certain percentage of the input energy. This portion of energy might be used for on-site channel monitoring of the WDDM.



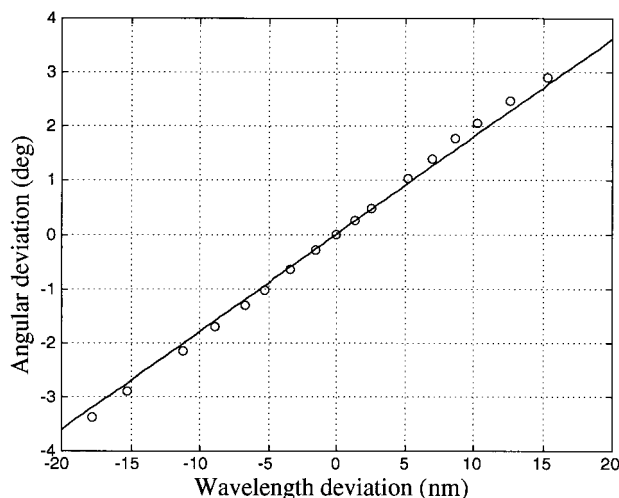


Fig. 4. Experimental results (circles) and theoretical expectations (curve) of the angular deviation as a function of the wavelength change at a center wavelength of 800 nm.

#### A. Four-Channel Wavelength-Division Demultiplexer

Figure 4 shows the measured dispersion of the WDDM. Theoretical results calculated by use of Eq. (2) are also shown in the figure as the solid curve. It is obvious that the experimental results are consistent with the theoretical expectations. The dispersion is found to be insensitive to the states of the input polarization. Figure 5 gives the measured diffraction efficiencies of the +1-order forward diffraction as a function of wavelength under different states of polarization. The diffraction efficiency is defined as the intensity of the +1-order forward diffraction divided by the intensity of the optical signal entering the WDDM (not the output waveguide grating). Actually, before the optical signal impinges upon the grating, it experiences losses of Fresnel reflection at the air-glass and the reflection-coating

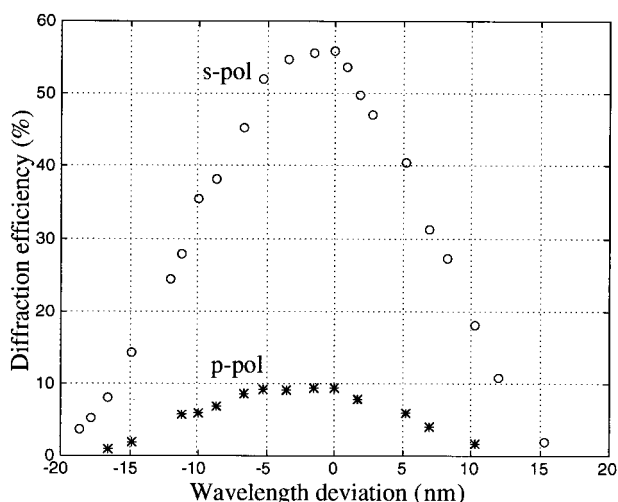


Fig. 5. Measured diffraction efficiency as a function of the wavelength change at a center wavelength of 800 nm under an *s*-polarization (*s*-pol) wave and a *p*-polarization (*p*-pol) wave for the WDDM.

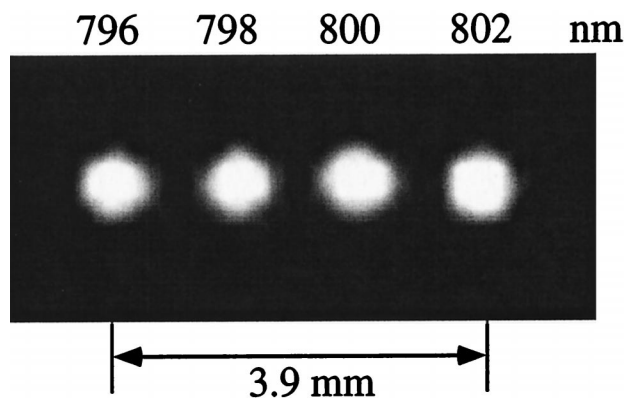


Fig. 6. CCD image of the light spots for the WDDM operating at 796, 798, 800, and 802 nm.

interfaces and absorption and scattering of the waveguiding glass plate. Therefore the actual diffraction efficiencies of the grating are higher than those given in Fig. 5. The 3-dB bandwidth of this device is determined to be 20 nm, which is close to the value given in Table 1. The discrepancy in diffraction efficiencies between the *p*-polarization (TM wave) and the *s*-polarization (TE wave) states shows that this device is polarization sensitive. Different boundary conditions that exist between the TE and the TM waves cause the polarization dependence of the radiation of the diffracted beam. Theoretical analysis with rigorous coupled-wave analysis is planned for another publication.

Figure 6 shows the experimental results for a four-channel WDDM operating at 796, 798, 800, and 802 nm, for which the bandwidth of the device can accommodate all four channels, as shown in Fig. 5, while maintaining a 2-nm wavelength separation. This image was taken with a CCD camera from the focal plane of a lens with a focal length of 20 cm. From Fig. 6 we can see that the four channels are completely separate. There is no interchannel cross talk observed in our experiment. With an aspheric lens it is possible to focus the light beams much more tightly and to couple them into standard multimode-fiber bundles-arrays and to obtain a less than 6-dB total insertion loss. This device can also be used as a WDM in the reciprocal direction.

#### B. Path-Reversed Substrate-Guided-Wave Optical Interconnect with Multiple Fan-Outs

To further increase the capacity and reduce the cost of the WDDM, we designed a path-reversed substrate-guided-wave-based WDDM with a multiple-fan-out feature. Figure 7 shows that  $N$  cascaded volume holographic gratings are integrated on the same waveguiding plate and that optical signals of different wavelengths zigzag within the plate and are coupled sequentially out of the substrate by the cascaded gratings. For each individual fan-out the dispersed wavelengths can be focused and coupled into optical fiber arrays. If each holographic grating is capable of separating  $M$  wavelengths, such a WDDM has a channel

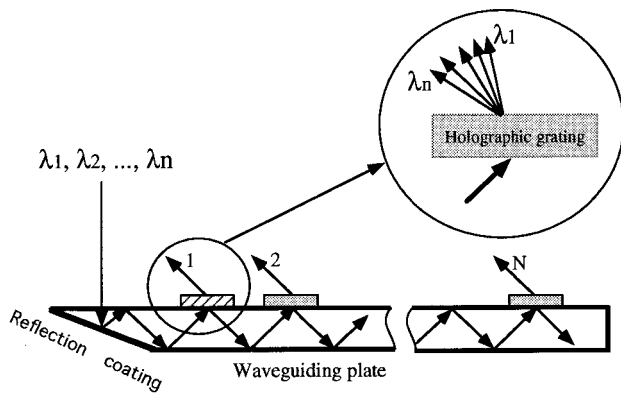


Fig. 7. Path-reversed substrate-guided wave optical interconnection with multiple-fan-outs for WDDM application.

capacity of  $N \times M$ , which is  $N$  times larger than that described in Section 2. An important issue that relates to this device is obtaining a uniform fan-out energy distribution; this subject is discussed elsewhere.<sup>34,35</sup>

Using the same grating parameters as mentioned above and a beveled waveguiding plate with a thickness of 3.2 mm, we sequentially recorded five cascaded holograms on the same substrate by using DuPont photopolymer film HRF 600 with a thickness of 20  $\mu\text{m}$ . Figure 8 shows a CCD image of the device operating at a center wavelength of 800 nm under  $s$  polarization. A three-dimensional intensity profile is shown in Fig. 8(b). The fan-out energy-distribution uniformity is measured to be within

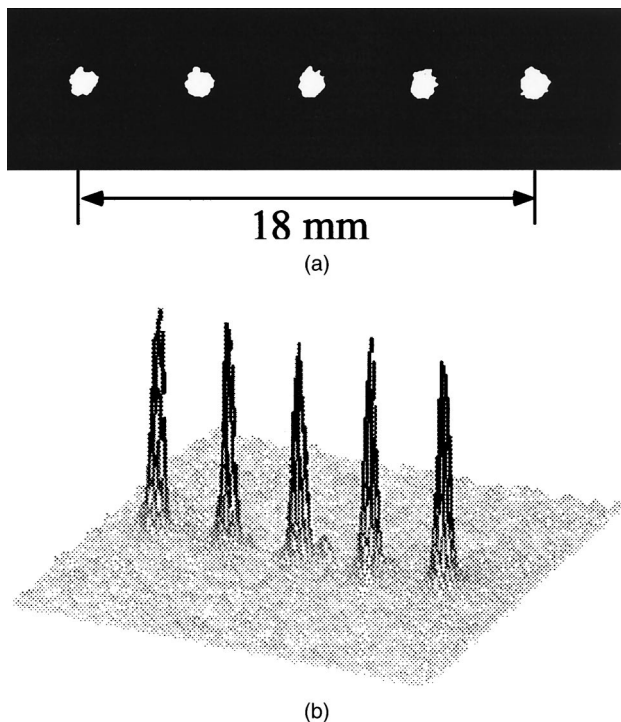


Fig. 8. Experimental results of a one-to-five fan-out WDDM operating at a center wavelength of 800 nm: (a) CCD image and (b) three-dimensional intensity profile.

$\pm 5\%$ . The overall efficiency<sup>34</sup> is measured to be 35%. For each individual fan-out four channels with a channel wavelength separation of 2 nm are also obtained, similar to those shown in Fig. 6. This large user-sharing capacity makes the device promising for data communications. One disadvantage of such a cascaded configuration is that the multiple-fan-out energy uniformity and the overall efficiency are not polarization independent because of the large discrepancy in the diffraction efficiencies of the  $p$  and the  $s$  polarizations.<sup>6</sup> When each individual cascaded hologram is recorded with the maximum diffraction efficiency it can be used as a multiport WDM. If the same device is used for both multiplexing and demultiplexing a compromise is needed between the fan-out energy-distribution uniformity for demultiplexing and the coupling efficiencies of the first few cascaded holograms for multiplexing.

#### 4. Summary

In this paper a novel, to our knowledge, multiwavelength photopolymer-based path-reversed substrate-guided-wave optical interconnect has been presented. The dispersion and the bandwidth of the guided-wave holograms have been analyzed. It has been shown that adjusting the incident angle and the diffraction angle of the path-reversed structure can enhance the dispersion. Incident angles larger than the critical angle of the substrate can be obtained if one edge of the waveguiding plate is beveled. The bulky waveguiding glass plate provides mechanical and environmental robustness. As dispersion occurs for the output holographic grating, the  $\text{TEM}_{00}$  mode profile of the dispersed optical signals of different optical wavelengths is retained well, and this also reduces difficulties in integration with fiber arrays-bundles.

In our experiment the DuPont photopolymer film HRF 600 $\times$ 001-20 (20  $\mu\text{m}$  thick) has been chosen for recording the holographic grating. The beveled angle of the waveguiding plate is  $\alpha = 22.5^\circ$ , and the diffraction angle of the holographic grating in air is designed to be  $45^\circ$ . The measured dispersion results are consistent with those of the theoretical analyses and are polarization insensitive. A bandwidth of 20 nm was obtained for such a polarization-sensitive device (in terms of the diffraction efficiency). A four-channel WDDM with wavelengths of 796, 798, 800, and 802 nm has been demonstrated with no channel cross talk. Furthermore, this structure can be incorporated with cascaded hologram arrays to obtain multiple fan-outs for increasing the user-sharing capacity and reducing the cost of the device. A one-to-five fan-out WDDM has been fabricated and exhibits an energy fluctuation that is within  $\pm 5\%$  under  $s$  polarization at a center wavelength of 800 nm. This path-reversed substrate-guided-wave optical interconnect appears promising for use as a WDDM in data communications. Its potential applications at 1550 nm are under investigation, and the results are planned for another publication.

This research is supported by the Ballistic Missile Defense Organization, the U.S. Army Space and Strategic Defense Command, the Center of Optoelectronics Science and Technology (COST), the Defense Advanced Research Projects Agency, the Office of Naval Research, the U.S. Air Force Office of Scientific Research Cray Research, DuPont, Lightpath, and the Advanced Technology Program (ATP) of the State of Texas.

## References

1. A. Pu and D. Psaltis, "High-density recording in photopolymer-based holographic three-dimensional disks," *Appl. Opt.* **35**, 2389–2398 (1996).
2. S. Reinhorn, Y. Amitai, and A. A. Friesem, "Compact planar optical correlator," *Opt. Lett.* **22**, 925–927 (1997).
3. S. Reinhorn, S. Gorodeisky, A. A. Friesem, and Y. Amitai, "Fourier transformation with a planar holographic doublet," *Opt. Lett.* **20**, 495–497 (1995).
4. J. Liu, C. Zhao, and R. T. Chen, "Implementation of optical perfect shuffle with substrate-guided wave optical interconnects," *IEEE Photon. Technol. Lett.* **9**, 946–948 (1997).
5. J. Liu, C. Zhao, R. Lee, and R. T. Chen, "Cross-link optimized cascaded volume hologram array with energy-equalized one-to-many surface-normal fan-outs," *Opt. Lett.* **22**, 1024–1026 (1997).
6. J. Liu, Z. Fu, and R. T. Chen, "Polarization sensitivity of photopolymer-based volume holograms for one-to-many surface normal optical interconnects," *Opt. Eng.* **37**, 660–665 (1998).
7. J. Liu and R. T. Chen, "A two-dimensional dual-wavelength routing network with 1-to-10 cascaded fanouts," *IEEE Photon. Technol. Lett.* **10**, 238–240 (1997).
8. M. M. Li and R. T. Chen, "Five-channel surface-normal wavelength-division demultiplexer using substrate-guided waves in conjunction with a polymer-based littrow hologram," *Opt. Lett.* **20**, 797–799 (1995).
9. M. K. Smit, "New focusing and dispersive planar component based on an optical phased array," *Electron. Lett.* **24**, 385–386 (1988).
10. H. Takahashi, S. Suzuki, K. Kato, and I. Nishi, "Arrayed-waveguide grating for wavelength division multi/demultiplexer with nanometer resolution," *Electron. Lett.* **26**, 87–88 (1990).
11. C. Dragon, C. H. Henry, I. P. Kaminow, and R. C. Kistler, "Efficient multichannel integrated optics star coupler on silicon," *IEEE Photon. Technol. Lett.* **1**, 241–243 (1989).
12. C. Dragon, "An  $N \times N$  optical multiplexer using a planar arrangement of two star couplers," *IEEE Photon. Technol. Lett.* **3**, 812–815 (1991).
13. C. Dragon, C. A. Edwards, and R. C. Kistler, "Integrated optics  $N \times N$  multiplexer on silicon," *IEEE Photon. Technol. Lett.* **3**, 896–899 (1991).
14. M. K. Smit and C. van Dam, "PHASAR-based WDM devices: principles, design and applications," *IEEE J. Select. Topics Quantum Electron.* **2**, 236–250 (1996).
15. K. O. Hill, Y. Fujii, D. C. Johnson, and B. S. Kawasaki, "Photosensitivity in optical fiber waveguides: application to reflection filter fabrication," *Appl. Phys. Lett.* **32**, 647–649 (1978).
16. B. S. Kawasaki, K. O. Hill, D. C. Johnson, and Y. Fujii, "Narrow-band Bragg reflectors in optical fibers," *Opt. Lett.* **3**, 66–68 (1978).
17. F. Bilodeau, D. C. Johnson, S. Theriault, B. Malo, J. Albert, and K. O. Hill, "An all-fiber dense-wavelength-division multiplexer/demultiplexer using photoimprinted Bragg gratings," *IEEE Photon. Technol. Lett.* **7**, 388–390 (1995).
18. I. Baumann, J. Seifert, W. Nowak, and M. Sauer, "Compact all-fiber add-drop multiplexer using fiber Bragg gratings," *IEEE Photon. Technol. Lett.* **8**, 1331–1333 (1996).
19. K. O. Hill and G. Meltz, "Fiber Bragg grating technology fundamentals and overview," *J. Lightwave Technol.* **15**, 1263–1276 (1997).
20. G. W. Neudeck, J. Denton, J. D. Schaub, R. Li, C. L. Schow, and J. C. Campbell, "A high speed Si photodiode by epitaxial lateral growth," paper presented at the Fifty-sixth Annual Device Research Conference, Charlottesville, Va., 22–24 June 1998.
21. C. Schow, J. Schaub, R. Li, J. Qi, and J. C. Campbell, "A 1 Gb/s monolithically integrated silicon NMOS optical receiver," *IEEE Quantum Electron.* (to be published).
22. S. Hu, J. Ko, and L. A. Coldren, "High-performance densely packed vertical-cavity photonic integrated emitter arrays for direct-coupled WDM applications," *IEEE Photon. Technol. Lett.* **10**, 766–768 (1998).
23. D. L. Huffaker and D. G. Deppe, "Multiwavelength, densely packed  $2 \times 2$  vertical-cavity surface-emitting laser array fabricated using selective oxidation," *IEEE Photon. Technol. Lett.* **7**, 858–860 (1996).
24. S. Y. Hu, J. Ko, O. Sjolund, and L. A. Coldren, "Optical crosstalk in monolithically integrated multiple wavelength vertical-cavity laser arrays for multimode WDM local area networks," *Electron. Lett.* **34**, 676–678 (1998).
25. Y. K. Tsai, Y. T. Huang, and D. C. Su, "Multiband wavelength-division demultiplexing with a cascaded substrate-mode grating structure," *Appl. Opt.* **34**, 5582–5588 (1995).
26. W. Gambogi, K. Steijn, S. Mackara, T. Duzik, B. Hamzavy, and J. Kelly, "HOE imaging in DuPont holographic photopolymers," in *Diffraction and Holographic Optics Technology*, I. Cindrich and S. H. Lee, eds., *Proc. SPIE* **2152**, 282–293 (1994).
27. U. Rhee, H. J. Caulfield, C. S. Vikram, and J. Shamir, "Dynamics of hologram recording in DuPont photopolymer," *Appl. Opt.* **34**, 846–853 (1995).
28. S. Piazzolla and B. K. Jenkins, "Holographic grating formation in photopolymers," *Opt. Lett.* **21**, 1075–1077 (1996).
29. H. J. Zhou, V. Morozov, and J. Neff, "Characterization of DuPont photopolymers in infrared light for free-space optical interconnects," *Appl. Opt.* **34**, 7457–7459 (1995).
30. R. R. A. Syms, *Practical Volume Holography* (Clarendon, Oxford, 1990).
31. J. E. Ludman, "Approximate bandwidth and diffraction efficiency in thick holograms," *Am. J. Phys.* **50**, 244–246 (1982).
32. H. Kogelnik, "Coupled wave theory for thick hologram gratings," *Bell Sys. Tech. J.* **13**, 2909–2947 (1969).
33. T. K. Gaylord and M. G. Moharam, "Analysis and applications of optical diffraction by gratings," *Proc. IEEE* **73**, 894–937 (1985).
34. J. Liu and R. T. Chen, "Substrate-guided-wave-based optical interconnects for multi-wavelength routing and distribution networks," *J. Lightwave Technol.* **17**, 354–361 (1999).
35. T. Nakaya, Y. Katoh, T. Kubota, and M. Takeda, "Diffraction efficiency of a grating coupler for an array illuminator," *Appl. Opt.* **35**, 3891–3898 (1996).